Ab Initio Atomic Thermodynamical Investigation on the Annealing Mechanisms of the Oxygen Defects in the Anatase TiO_2

Zhijun Cheng, Tingyu Liu[*], *Chenxing Yang and Haixiu Gan*

College of Science, University of Shanghai for Science and Technology, Shanghai 200093, China

Jianyu Chen

Key Laboratory of Materials for High Power Laser, Shanghai Institute of Optics and Fine Mechanics, Chinese Academy of Sciences, Shanghai 201800, China

Feiwu Zhang

Nanochemistry Research Institute, Curtin University, GPO Box U1987, Perth, WA 6845, Australia

Abstract

In the framework of the *ab initio* Atomic Thermodynamics, the preliminary analysis of the annealing mechanisms of the oxygen defects in anatase TiO_2 has been done by investigating the influence of the annealing treatment under representative conditions on three typical oxygen defects, that is, oxygen vacancy, oxygen adsorption and oxygen interstitial, all of which exist during the annealing treatment by the defect chemistry, therefore, should be explored independently. Our results in this study agree well with the related experiments findings including the recent discoveries, e.g., we find that the type of the molecular ion of the adsorbed O_2 can also be determined by the initial orientation of O_2 relative to the surface (101). However, the critical annealing conditions under which the

*Corresponding author. Email: liutyyxj@163.com Tel: 086-021-65667034

dominant oxygen defects would begin to convert to another one have not been found out due to the drawback of the current research scheme and we propose that this flaw could be compensated by studying the kinetics of the reactions, which may be the major task in the next stage of this research.

Keyword: Anatase; Annealing treatment; Oxygen defects; Ab initio atomic thermodynamics

1. Introduction

Recently, it has been confirmed that the reduced anatase TiO_2 is a very effective visible-light photocatalyst [1] and the key factors are attributed to the shallow donor states in the band gap produced by the oxygen vacancies[2]. When anatase TiO_2 is used as the gas sensors, the working mechanism is closely related to the presence of the oxygen vacancies as well[3]. On the other hand, in 2011, Vinodkumar Etacheri et al [4] first reported a high temperature stable and visible-light active anatase photocatalyst: oxygen rich titania, which is free of dopant and can remain the anatase phase up to 900 ^{o}C. The authors proposed that it is the high concentrations of interstitial O in the anatase that lead to the unique properties of this kind of titania. Since the oxygen defects could play significant role in improving the performance of the anatase TiO_2, issues related to these chemical defects are becoming the research hotspots, such like the effect of annealing process on those point defects.

Comparing with other process during the crystal growth, annealing treatment is such a process closely related to the thermal motions of the point defects, involving the generation, elimination and transformation between these defects. The oxygen vacancies in anatase, for example, can be reduced after the as-grown TiO_2 grown by a chemical vapor transport reaction method were annealed in oxygen atomsphere of 1.0 MPa at relatively high temperature[5]. In contrast, under normal synthesis conditions, high temperature annealing treatment of TiO_2 would always generate the oxygen vacancies[6,7]. That is to say, it closely depends on the annealing temperature and the oxygen partial pressure in the atmosphere. Should the oxygen species incorporate into[4,8] or escape from the

anatase TiO_2? Which indicates quite complicated physical and chemical reaction processes.

However, current experimental researches on the annealing treatment are mainly concentrated on the exploration of the annealing technology[9,10] and the analysis of the experimental results is still at the qualitative level lacking of the understanding of the microscopic kinetic mechanism of the defect movements during the annealing process, which leads to the difficulty in precisely predicting the influence of certain annealing process on the physical properties of the anatase TiO_2 and in controlling the proper annealing conditions to produce the desired type and concentration of the oxygen defect in this material. With the rapid development of the supercomputer, fortunately, the material simulation technology can bridge this serious shortage and can obtain valuable information at the atomic and electronic levels. Therefore, in this paper, by the first-principle calculations we will theoretically investigate and find out the microscopic dynamics mechanism of the oxygen defects in the anatase TiO_2 with attention mainly focused on the effect of the annealing treatment on three typical oxygen defects: oxygen vacancy, interstitial oxygen and molecular oxygen adsorbed on the surface, all of which play the fundamental roles in the generation or transformation of the oxygen defects during the heat treatment.

2. Theories and methods

The first-principle calculations are based on the Density Functional Theory (DFT) using the plane wave pseudopotential method[11,12] implemented in the Vienna Ab-initio Simulation Package (VASP) codes[13]. The detailed computational parameters such as the cutoff energy, the valence configurations and the pseudopotential of the Ti and O ions, the supercell size for simulating the bulk and so on, can be found in our previous study on the anatase[2]. All surfaces were modeled by slab geometries with a vacuum of 10 Å[14] between slabs. In order to check the dependence on the concentration of the defects, we used slabs of four[15,16] TiO_2 layers with two different surface unit cell: c (1×2), dimension 1×2 in the $[\bar{1}01]$ and $[010]$ directions, and c (1×3) containing 96 and

144 atoms, respectively, for surface (101). Correspondingly, the Monkhorst-Pack k-point sampling is set as 2×3×1 and 2×2×1 for surface c (1×2) and c (1×3). During the geometry optimizations, the atoms in the bottom layer were fixed to their bulk positions to simulate the presence of the bulk underneath and others were free to relax until the computations reached the desired convergence standard[2]. Finally, as the ground state of the oxygen molecule is triplet[17], so we carried out the spin-polarized calculations for the adsorption of O_2 on the anatase surface.

The influence of the annealing treatment on the oxygen defects were studied by the Ab Initio Atomistic Thermodynamics, which combines the first-principles calculations of the atomic (and electronic) structure with concepts of thermodynamics and has been used to research the defects in semiconductors and semiconductor surfaces and interfaces for a long time[18,19,20]. Through the oxygen chemical potential uniquely describing the O_2 gas environment, we can take into account the effect of annealing conditions, i.e., the temperature T and the oxygen partial pressure P_{O_2}. Within the ideal gas approximation, the oxygen chemical potential reflecting the availability of the oxygen species can be obtained by the following formula[18]:

$$\mu_o ?\mathrm{T}, p? = \frac{1}{2}[E_{O_2}^{total} + \mu_{O_2}(T, p^0) + K_B T \ln(P_{O_2}/p^0)] \tag{1}$$

P^0=1 bar and the internal degrees of freedom of the O_2 molecule (vibrations and rotations) are included in the $\mu_{O_2}(T, p^0)$; the total energy of the isolated oxygen molecule $E_{O_2}^{total}$ can be computed by DFT. Usually, the reference point of the oxygen chemical potential is set as the half of the total energy of the O_2 molecule, $\frac{1}{2}E_{O_2}$, and hence formula (1) can be rewritten as[21]:

$$\Delta\mu_o(T, P_{O_2}) = \mu_o(T, P_{O_2}) - \frac{1}{2}E_{O_2} = \frac{1}{2}\{\Delta G_{O_2}^{gas}(T, P^0) + K_B T \ln(P/P^0)\} + \delta\mu_O^0 \tag{2}$$

$$\Delta G_{O_2}^{gas}(T, P^0) = G_{O_2}^{gas}(T, P^0) - G_{O_2}^{gas}(T^0, P^0) \tag{3}$$

$$\delta\mu_O^0 = \frac{1}{2}[E_{TiO_2} - E_{Ti} - \Delta H_f^0(TiO_2)] - \frac{1}{2}[E_{O_2} + T^0 S_{O_2}^{gas}(T^0, P^0)] \tag{4}$$

Where T^0=298.15K, P^0=1bar; E_{TiO_2} (E_{Ti}) is the formation energy of anatase TiO_2 (hcp Ti) per molecular formula; $\Delta H_f^0(TiO_2)$ [22] and $S_{O_2}^{gas}(T^0, P^0)$ [23] is the formation enthalpy for TiO_2 and the O_2 gas entropy under the standard conditions respectively. The correction term $\delta\mu_o^0$ in (2) matches the origin of the experimental variation of the oxygen chemical potential and the reference point in our theoretical estimates.

However, the oxygen chemical potential cannot be arbitrary and should follow the equilibrium growth conditions and some other limitations[24] to ensure the titanium-oxygen stable phase is the anatase TiO_2 crystal, rather than other alternative phase such as TiO, Ti_2O_3 or even hcp Ti and O_2 molecule. For all of the annealing conditions considered here, yet this constrain on the oxygen chemical potential is fully satisfied.

After obtaining the oxygen chemical potential, we can derive some critical thermodynamic quantities for the formation of the relevant oxygen species. In this respect, we adopt the same approximation as in the research of (La, Sr)MnO_{3-x} cathode materials by Mastrikov et al[21], that is, the changes of vibrational entropy in the solid are neglected and thus only states comprising gaseous O_2 exhibit a temperature-dependent Gibbs free energy contribution. As a result, differences between Gibbs energies for bulk crystals or slabs (including defects and adsorbates) could be replaced with the differences in the total energy from the DFT. The Gibbs free energy of reaction for the formation of oxygen vacancy with charge state +q (V_o^{+q}) is defined as:

$$\begin{aligned}\Delta G_f[V_o^{+q}] &= E_{tot}[V_o^{+q}] - E_{tot}[0] + \mu_o + q\times[E_F + E_V + \Delta V] \\ &= E_{tot}[V_o^{+q}] - E_{tot}[0] + \mu_o + q\times[E_F + E_V + \Delta V] - \frac{1}{2}E_{O_2} + \frac{1}{2}E_{O_2} \\ &= (E_{tot}[V_o^{+q}] + \frac{1}{2}E_{O_2} - E_{tot}[0]) + (\mu_o - \frac{1}{2}E_{O_2}) + q\times[E_F + E_V + \Delta V] \\ &= \Delta E_f^{DFT}(V_O^{+q}) + \Delta\mu_O(T, P_{O_2}) + q\times[E_F + E_V + \Delta V]\end{aligned}$$

(5)

The detailed meaning of each term can be found in [2] and we should note that (5) can be applied

to both the bulk and the surface.

Similarly, the Gibbs formation energy of the interstitial oxygen can be represented as:

$$\begin{aligned}\Delta G_f[\mathrm{O}_i^{-q}] &= E_{tot}[O_i^{-q}] - E_{tot}[0] - \mu_o - q\times[E_F + E_V + \Delta V] \\ &= E_{tot}[O_i^{-q}] - E_{tot}[0] - \mu_o - q\times[E_F + E_V + \Delta V] - \frac{1}{2}E_{O_2} + \frac{1}{2}E_{O_2} \\ &= (E_{tot}[O_i^{-q}] - \frac{1}{2}E_{O_2} - E_{tot}[0]) - (\mu_o - \frac{1}{2}E_{O_2}) - q\times[E_F + E_V + \Delta V] \\ &= \Delta E_f^{DFT}(O_i^{-q}) - \Delta\mu_O(T, P_{O_2}) - q\times[E_F + E_V + \Delta V]\end{aligned}$$

(6)

The Gibbs free energy of O_2 adsorption on the surface[21] can be written analogously:

$$\begin{aligned}\Delta G_{\mathrm{ads}}[O_2] &= E_{tot}[O_2] - E_{tot}[0] - 2\mu_o \\ &= E_{tot}[O_2] - E_{tot}[0] - 2\mu_o - E_{O_2} + E_{O_2} \\ &= (E_{tot}[O_2] - E_{O_2} - E_{tot}[0]) - (2\mu_o - E_{O_2}) \\ &= \Delta E_{ads}^{DFT}(O_2) - 2\Delta\mu_O(T, P_{O_2})\end{aligned}$$

(7)

3. Results and discussions

3.1. Oxygen vacancies

In order to compare the experimental results, we consider several typical annealing conditions[8]. Two different oxygen partial pressure, 1atm and 10^{-4}Torr, are adopted to model the O-rich and O-poor gas atmosphere with the annealing temperature T changing from 200 ℃ to 500 ℃. The calculated oxygen chemical potential can be found in Fig.1. Under different annealing conditions, the Gibbs formation energies of oxygen vacancies in bulk as a function of the Fermi level are plotted in Fig. 2 (a) and (b).

From the Fig.2, it can be easily found that under the fixed gas partial pressure the Gibbs formation energy of the oxygen vacancy will decrease if the annealing temperature increases. Likely, with the temperature fixed, the lower oxygen partial pressure will lead to the formation of the oxygen

vacancy much easier. As a result, to maintain certain concentration of the oxygen vacancy in the anatase, the oxygen partial pressure must simultaneously decrease if the annealing treatment is carried out at lower temperature. This deduction is based on the following physical facts: when the oxygen partial pressure P_{O_2} get lower (or the temperature become higher), as shown in Fig.1., the chemical potential of the O_2 in the atmosphere will reduce, leading to the increase in the reaction rate at which the oxygen spread from the crystal to the gas, i.e., the formation energy of the oxygen vacancy will drop to some extent. This is consistent with the secondary ion mass spectrometers (SIMS) results of the oxygen surface exchange on the gadolinia doped ceria by Lane et al[25], who found that after the annealing treatment in the ^{18}O isotope enriched gas the concentration of ^{18}O within the sample decreases as the P_{O_2} decreases, i.e., the reverse process of the incorporation become enhanced by the reduction of the P_{O_2}.

The location in the band gap of the thermodynamic transition level[26] between the +2 and 0 vacancies, as shown in Fig.2 by the small arrow, is independent on the annealing conditions. So the charge state of the oxygen vacancy is only the function of the Fermi level, which is determined by the overall electrical neutrality condition of the crystal and the surrounding chemical environment[27].

Recently, it has been distinctly proven by the STM experiment[28] and the DFT calculations[15,29] that the oxygen vacancy is energetically more stable at the subsurface site than on the surface in the case of anatase TiO_2. On the other hand, lots of experiments such as the conductivity measurements[24] have confirmed that the anatase behave as a n-type semiconductor[3], implying that the Fermi level is near the bottom of the conduction band and so the charge state of the oxygen vacancy is most likely zero. Considering the above findings, we had better investigate the effect of the annealing treatment only on the neutral oxygen vacancy at the subsurface site of anatase TiO_2

(101) surface, a majority surface[30] of the anatase crystal, which seems more practical and meaningful.

After the structure is optimized, the slab geometries for simulating the (101) surface with a subsurface neutral oxygen vacancy are shown in Fig.3. In the case of surface c(1×2), the variations of the Gibbs formation energies of the oxygen vacancy with the Fermi level under various annealing conditions are depicted in Fig.4.

When comparing the Gibbs formation energies of the neutral oxygen vacancy in bulk with that in subsurface, as illustrated in Fig.2 and Fig.4 respectively, we can draw an interesting and significant conclusion that is indeed found in the phase-transformation related experiments. When the oxygen partial pressure is 1 atm or 10^{-4} Torr, the Gibbs formation energy of the subsurface vacancy is always less than 4.0 eV or 3.6 eV, respectively, at any temperature considered here. In contrast, at any temperature the formation energy of the vacancy in bulk is always larger than 4.1 eV for 1 atm or 3.6 eV for 10^{-4} Torr. No matter what the annealing condition is, in a word, the oxygen vacancy is energetically more favorable at the subsurface site than in the bulk indicating that under the reducing annealing conditions the formation of the oxygen vacancy in the anatase TiO_2 crystal may firstly undertake at the surface. On the other hand, it is considered that the process of anatase to rutile phase transformation involves the breaking of two of the six Ti-O bonds in anatase, usually accompanying with the formation of the oxygen vacancy[4] and lots of experimental results have confirmed that the rutile formation starts at the anatase surface[31,32] or interface between the anatase particle[33,34]. As a result, both the theoretical and the experimental results have consistently confirmed that the initial reaction step of the reduction of the anatase may occur at the anatase surface during the annealing treatment.

3.2. Adsorption of O_2

In order to completely and systematically explore the annealing mechanisms of the oxygen

defects in anatase TiO_2, we need to investigate the effect of the annealing treatment on the adsorption of O_2 on the surface, i.e., the interaction between the oxygen molecule and the surface. Since the subsurface oxygen vacancy which is a kind of dominant surface defect has great influence on the surface reactivity of anatase TiO_2[35], it is essential to consider the adsorption of O_2 on the surface containing the subsurface oxygen vacancy. Here, we take into account all of the typical orientations of O_2 such as $[\bar{1}01]$, $[010]$ and $[101]$ and the most preference adsorption site on the surface relative to the subsurface defect is chosen the same as that in the literature[36] which discusses the adsorption of oxygen molecule on the surface (101) with a subsurface oxygen vacancy and all of the possible adsorption sites are compared, but only one of the orientations of O_2, $[010]$, is probed. The initial bond length of O_2 is 1.208 Å[23] and the initial distance between the molecule and the surface is 2.0 Å. The optimized structure can be found in Fig.5 (a) and (c).

From Fig. 5 (a) we can notice that there is a special phenomenon appearing when the O_2 along $[\bar{1}01]$ interacts with the surface (101), which is not observed at all in [36]. This unique appearance is that the O_2 would occupy the lattice site of the O_{2c} at the surface. The detailed process of the atomic relaxation, as shown in Fig. 5 (b), is: (1) the oxygen atom nearest to the vacancy hold the site of the defect forming a new temporary vacancy; (2) the O_{2c} at the surface take over the site of the new defect and a surface oxygen vacancy appear simultaneously; (3) at last, O_2 occupy the site of the surface vacancy. In a word, in this situation the subsurface vacancy would not steadily exist and greatly prompt the adsorption of the O_2 on the surface. This can be further explained as following by the analysis of change of the important structural parameters: bond length of the O_2. In Fig. 5 (a), the bond length of O_2 has increased to 1.386 Å indicating that the oxygen molecule has become the peroxide species[21,36] (O_2^{2-}, O-O $\approx$ 1.48 Å) and the excess electrons of the oxygen vacancy have totally transferred to O_2. This results are consistent with many experimental and theoretical discoveries that the adsorbed oxygen on anatase surface functions as a very efficient

electron scavenger[8,36]. Nevertheless, if O_2 is adsorbed on a perfect surface (101), then the bond length of O_2 merely increases by 0.017 Å and meanwhile the molecule move outward by 0.37 Å from the surface.

When the vertical O_2 is adsorbed on the surface (see Fig.5 (c)), the bond length of the molecule increase to 1.262 Å, around the typical bond length of the superoxide species (O_2^-, O-O $\approx$ 1.33 Å), and the distance between the molecule and the surface decreases to 1.79 Å, signifying that the chemisorption has occurred since the bond length of O-Ti in the bulk is about 1.9 Å. The appearance of the superoxide species have proven that the molecular species of the adsorbed O_2 is determined not only by the ratio of the number of O_2 to that of the vacancy as pointed out by Ulrich Aschauer et al. who consider that the peroxide species are stable when the number of O_2 is less or equal the number of the defects[36], but also by the orientation of O_2 relative to the surface.

Finally, the influence of the annealing treatment on the adsorption of O_2 on the anatase TiO_2 surface (101) could be clearly seen from the Gibbs adsorption energy under various annealing conditions, as shown in Fig.6. The Gibbs adsorption energy of the O_2 along $[\bar{1}01]$ is always negative, i.e., in this case the adsorption reaction is an exothermic process and hence it is effortless for O_2 in the direction of $[\bar{1}01]$ to be absorbed on the surface. Inversely, the positive sign of the absorption energy of the O_2 in $[101]$ states that this is an endothermic process and it's hard for this reaction to take place. Besides, according to[36], the adsorption energy of the O_2 along $[010]$ is -2.01 eV and so this process is also quite possible. Since both $[010]$ and $[\bar{1}01]$ are parallel to the surface (101), so we could draw the conclusion that the adsorption of O_2 whose orientation is parallel to the surface should be more favorable. This may be due to the following two reasons. First, it's known to all that the highest occupied molecular orbital (HOMO) of O_2 in the ground state is π^* and so the electron cloud is perpendicular to the axes of the oxygen molecule. Besides, the upper valence band of anatase TiO_2 is due to the π bonding from the hybridization of O p_π and Ti d_{xz}

(or d_{yz})[2]. So, all of these facts result in the bond making between the horizontal O_2 and the Ti much easier and steadier than that of the vertical O_2, which also arouses the difference in the adsorption energy between the two kinds of O_2.

3.3. Interstitial oxygen

The last type of the oxygen defect we are concerned about is the interstitial oxygen, which usually takes part in the chemical reaction of the oxygen defect during the annealing treatment. Besides, since the key factor bringing about the remarkable characteristic of the oxygen rich titania is the formation of the interstitial oxygen, as discussed in [4], we also would like to explore the improvement of the physical properties by this oxygen defect in the atomic and electronic level. The relaxed structural model for simulating the interstitial oxygen is shown in Fig. 7.

From Fig. 7, we can see that the distinct change in the geometry is that the interstitial oxygen has approached to the neighbor oxygen at the lattice site to form a molecular ion, with the bond length of 1.447 Å, indicating that the molecular ion is just the peroxide species. Interestingly, it has been found that the interstitial oxygen in the bulk[24] would be stable in the form of molecular ion as well. Moreover, the motion modes of the ions in the surface around the oxygen defect during the optimizing of the structure are the same as that in the bulk, i.e., the ions will displace outward from the molecular ion, which may result in the increase in the lattice parameters a as found in[4] when the concentration of interstitial oxygen become high enough.

The influence of the annealing treatment on the interstitial oxygen is examined in terms of the Gibbs formation energy under various conditions and the results are described in Fig. 8, which illustrates that the preferable annealing conditions for the interstitial oxygen are an oxygen rich atmosphere and relative lower temperature. This results can also be acquired by analyzing the O_2:Ti

ration of the oxygen rich TiO_2, which decreases as the calcinations temperature increases[4], e.g., the O_2:Ti rations of the composition $2H_2O_2$-TiO_2 after annealing treatment at 600 ℃, 700 ℃ and 900 ℃ are 2.56, 2.54 and 2.50 respectively.

Unfortunately, in the thermodynamics picture we could not pick out the critical annealing conditions under which the dominant oxygen defects should begin to convert to another one, because the Gibbs formation energies of oxygen vacancy under all of the annealing conditions considered here are above 3.0 eV and conversely that of the interstitial oxygen are always less than 3.0 eV. However, it's no doubt that the favorable annealing conditions for the interstitial oxygen and the oxygen vacancy should be oxygen rich and oxygen poor atmosphere respectively, meaning that at certain value of the oxygen partial pressure the Gibbs formation energy of interstitial oxygen should be higher than that of the oxygen vacancy. This failure may be caused by the shortage of the reaction thermodynamics and should be offset by the reaction kinetics analysis which focuses on some key physical quantities such as the adsorption potential barrier, diffusion potential barrier, pathway of the incorporation and so on. But these calculations require so much computational resources that it's impossible for us to complete in the short run.

The various plots of the electronic density of states (DOS) of the surface (101) with interstitial oxygen are shown in Fig. 9. It's worth noting that the molecular ion caused by the interstitial oxygen has important contribution to the top of the valence band, leading to the reduction of the band gap. When the concentration of the interstitial oxygen increases, this effect may be greatly enhanced and finally the band gap will be small enough to give rise to the adsorption of the visible light. As already proposed in[4], this should be the reason why the oxygen rich titania can be qualified as the visible-light photocatalyst.

4. Conclusions

To sum up, through the Ab Initio Atomic Thermodynamics we have intensively discussed the influence of the annealing treatment on three typical oxygen defects, i.e., oxygen vacancy, adsorbed oxygen and the interstitial oxygen, all of which play primary roles in the defect chemistry of the thermal treatment. Although in this research scheme, i.e., the thermodynamics picture, which ignores some important physical quantities such as the adsorption and diffusion potential barriers, we fail to the critical annealing conditions under which the dominant oxygen defects could begin to convert to another one, yet our researches have already laid solid foundations for the further investigation of the annealing mechanism of the oxygen defects in anatase TiO_2.

The main conclusions of this work have been listed below:

(1) The lower oxygen partial pressure and the higher annealing temperature will both lead to the formaton of the oxygen vacancy much easier, consistent with the secondary ion mass spectrometers (SIMS) results. As a result, to maintain certain level of the oxygen vacancy in the anatase, the oxygen partial pressure must simultaneously decrease if the thermal treatment is carried out at lower temperature.

(2) Whatever the annealing condition is, the oxygen vacancy is easier to form at the surface than in the bulk indicating that the reduction reaction may firstly undertake at the surface during the annealing treatment, which is consistent with the phase transformation experiments.

(3) The types of the molecular species of the adsorbed O_2 are subject to the ratio of the number of the O_2 to that of the vacancy, as well as the orientation of O_2 relative to the surface.

(4) Under any annealing conditions, the adsorption of O_2 whose orientation is parallel to the surface should be more favorable.

(5) The preferable annealing conditions for the interstitial oxygen are the oxygen rich atmosphere and relative lower temperature. This result has also be confirmed in the study of the oxygen rich TiO_2 by analyzing the O_2:Ti ration at various calcinations temperatures.

(6) The molecular ion, peroxide species, caused by the interstitial oxygen has important contribution to the top of the valence band and lead to the reduction of the band gap.

Acknowledgment

This work is supported by the Innovation Fund Project for Graduate Student of Shanghai (JWCXSL1002), the Foundation of Shanghai Municipal Education Committee (Grant No. 09YZ210) and the Shanghai Leading Academic Discipline Project (S30502).

References

[1] I. Justicia, P. Ordejon, G. Canto, J. L. Mozos, J. Fraxedas, G. A. Battiston, R. Gerbasi, A. Figueras, Adv. Mater., 14 (2002), pp. 1399-1402.

[2] Z. J. Cheng, T. Y. Liu, C. X. Yang, H. X. Gan, F. W. Zhang, J. Y. Chen, J. Phys. Chem. Solids, 73 (2012), pp. 302-307.

[3] N. Savage, B. Chwieroth, A. Ginwalla, B. R. Patton, S. A. Akbar, P. K. Dutta, Sensor Actuat. B, 79 (2001), pp. 17-27.

[4] V. Etacheri, M. K. Seery, S. J. Hinder, S. C. Pillai, Adv. Funct. Mater., 21 (2011), pp. 3744-3752.

[5] T. Sekiya, K. Ichimura, M. Igarashi, S. Kurita, J. Phys. Chem. Solids, 61 (2000), pp. 1237-1242.

[6] G.R. Torres, T. Lindgren, J. Lu, C. G. Granqvist, S. E. Lindquist, J. Phys. Chem. B, 108 (2004), pp. 5995-6003.

[7] Y. Lida, S. Ozaki, J. Am. Ceram. Soc., 44 (1961), p. 120.

[8] J. C. Yu, J. Lin, D. Lo, S. K. Lam, Langmuir, 16 (2000), pp. 7304-7308.

[9] J. C. Gao, X. W. Tan, Y. Wang, J. Zhou, J. Funct. Mater. Devic., 113(2007), pp. 485-489. (In chinese)

[10] D. R. Xu, X. G. Xiao, C. Z. Wang, Y. Q. Zhang, D. Zhang, X. X. Gao, Y. L. Liu, High Power Laser Part. Beams, 19(2007), pp. 1390-1394. (In chinese)

[11] M. C. Payne, M. P. Teter, D. C. Ailan, T. A. Arias, J. D. Joanopouios, Rev. Mod. Phys, 64(1992), pp. 1045-1097.

[12] M. D. Segall, P. J. D. Lindan, M. I. J. Probert, C. J. Pickard, P. J. Hasnip, S. J. Clark, M. C. Payne, J. Phys. : Condens. Matter, 14(2002), pp. 2717-2744.

[13] G. Kresse, J. Furthmüller, Comput. Mater. Sci, 6(1996), p. 15.

[14] E. Finazzi, C. D. Valentin, A. Selloni, G. Pacchioni, J. Phys. Chem. C, 111(2007), pp. 9275-9282.

[15] H. Z. Cheng, A. Selloni, J. Chem. Phys., 131(2009), p. 054703.

[16] M. Lazzeri, A. Vittadini, A. Selloni, Phys. Rev. B, 63(2001), p. 155409.

[17] L. Zhang, H. F. Ji, Y. K. Lei, W. Xiao, Appl. Surf. Sci., 257(2011), pp. 8402-8408.

[18] J. K. Norskov, M. Scheffler, H. Toulhoat, Mrs Bull., 31(2006), pp. 669-674.

[19] K. Reuter, C. Stampfl, M. Scheffler, Handbook of Materials Modeling, Vol. 1, Edited by S. Yip (Springer, Berlin, 2005), pp. 149-194.

[20] W. X. Li, C. Stampfl, M. Scheffler, Phys. Rev. Lett., 90(2003), p. 256102.

[21] Y. A. Mastrikov, R. Merkle, E. Heifets, E. A. Kotomin, J. Maier, J. Phys. Chem. C, 114(2010), pp. 3017-3027.

[22] D. R. Lide, ed., CRC Handbook of Chemistry and Physics, 90th Edition (Internet Version 2010).

[23] M. W. Chase, NIST-JANAF Thermochemical Tables; American Chemical Society: Washington DC, 1998.

[24] S. Na-Phattalung, M. F. Smith, K. Kim, M. H. Du, S. H. Wei, S. B. Zhang, S. Limpijumnong, Phy. Rev. B, 73(2006), p. 125205.

[25] J. A. Lane, J. A. Kilner, Solid State Ionics, 136-137 (2000), pp. 927-932.

[26] C. G. Van de Walle, J. Neugebauer, J. App.l Phys., 95(2004), pp. 3851-3879.

[27] J. M. Sullivan, S. C. Erwin, Phys. Rev. B, 67(2003), p. 144415.

[28] Y. B. He, O. Dulub, H. Z. Cheng, A. Selloni, U. Diebold, Phy. Rev. Let., 102(2009), p. 106105.

[29] H. Z. Cheng, A. Selloni, Phys. Rev. B, 79(2009), p. 092101.

[30] A. Vittadini, M. Casarin, A. Selloni, Theor. Chem. Acc., 117(2007), pp. 663-671.

[31] M. R. Ranade, A. Navrotsky, H. Z. Zhang, J. F. Banfield, S. H. Elder, A. Zaban, P. H. Borse, S. K. Kulkarni, G. S. Doran, H. J. Whitfield, P. Natl. Acad. Sci. U. S. A., 99(2002), pp. 6476-6781.

[32] J. Zhang, M. J. Li, Z. C. Feng, J. Chen, C. Li, J. Phys. Chem. B, 110(2006), pp. 927-935.

[33] A. A. Gribb, J. F. Banfield, Am. Mineral., 82(1997), pp. 717-728.

[34] J. Zhang, Q. Xu, Z. C. Feng, M. J. Li, C. Li, Angew. Chem. Int. Ed., 47(2008), pp. 1766-1769.

[35] U. Ascharer, Y. B. He, H. Z. Cheng, S. C. Li, U. Diebold, A. Selloni, J. Phys. Chem. C, 114(2010), pp. 1278-1284.

[36] U. Aschauer, J. Chen, A. Selloni, Phys. Chem. Chem. Phys., 12(2010), pp. 12956-12960.

Figure captions

Figure 1 Calculated oxygen chemical potentials, referenced to the half of the total energy of the oxygen molecule, under various annealing conditions.

Figure 2 Gibbs formation energies of oxygen vacancies in bulk as a function of the Fermi level, under the annealing conditions of O-rich (a) and O-poor (b) and different temperatures shown by the color of the line (black: 200℃; red: 300℃; blue: 400℃; green: 500℃). The slope of the line is an indication of the charge state of the defect. The Fermi energy, referenced to the top of the valence band, is all the way to the experimental band gap. The vertical dotted line is the calculated band gap at the G (the center of the brillouin zone). The thermodynamic transition level between the two kinds of oxygen vacancies is shown as well.

Figure 3 Slab models and O-vacancy sites in this work. (a) surface c(1×3). (b) surface c (1×2). Oxygen and Ti atoms are red and blue, respectively.

Figure 4 Gibbs formation energies of the subsurface neutral oxygen vacancy in the surface (101) under different annealing conditions. The detailed description can be found in the caption of Fig. 2.

Figure 5 Slab geometries for simulating the adsorption of O_2 on the surface (101) containing a subsurface oxygen vacancy. (a): optimized structure for the adsorption of O_2 whose initial orientation is in the direction of $[\bar{1}01]$; (b): the detailed process of the atomic movement during the relaxation, shown in the initial structure; (c) the adsorption of O_2 along $[101]$. The molecular ions are highlighted by the ellipses. Oxygen and Ti atoms are red and blue, respectively.

Figure 6 Gibbs adsorption energies of the adsorption of O_2 on the surface (101) with a subsurface oxygen vacancy under various typical annealing conditions. (a) and (b) are for the case of the O_2 along $[\bar{1}01]$ with (c) and (d) for O_2 in $[101]$. The detailed description can also be found in the caption of Fig. 2.

Figure 7 Optimized slab model of the surface (101) having a interstitial oxygen. The molecular ions are highlighted by the ellipses and the O and Ti are red and blue, respectively.

Figure 8 Gibbs formation energy of the interstitial oxygen under various annealing conditions. The detailed description can also be found in the caption of Fig. 2.

Figure 9 Plots of the electronic density of states for surface (101) containing an interstitial oxygen. (1) is the total density of states (TDOS); (2) and (3) are the site decomposed local partial density of states (LPDOS) of Ti and O in bulk, respectively; (4) is the LPDOS of the Ti bonding with the molecular ion; (5) is the LPDOS of the O_2^{2-}; (6) and (7) are the LPDOS of the Ti and O in the surface, respective. The energy is referenced to the top of the valence band, which is also supposed to be equal to the Fermi level, E_f.

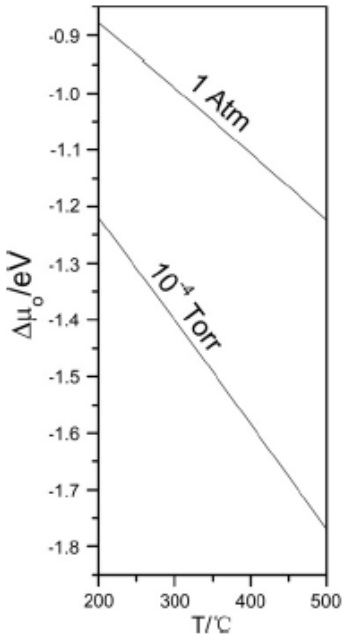

Figure 1

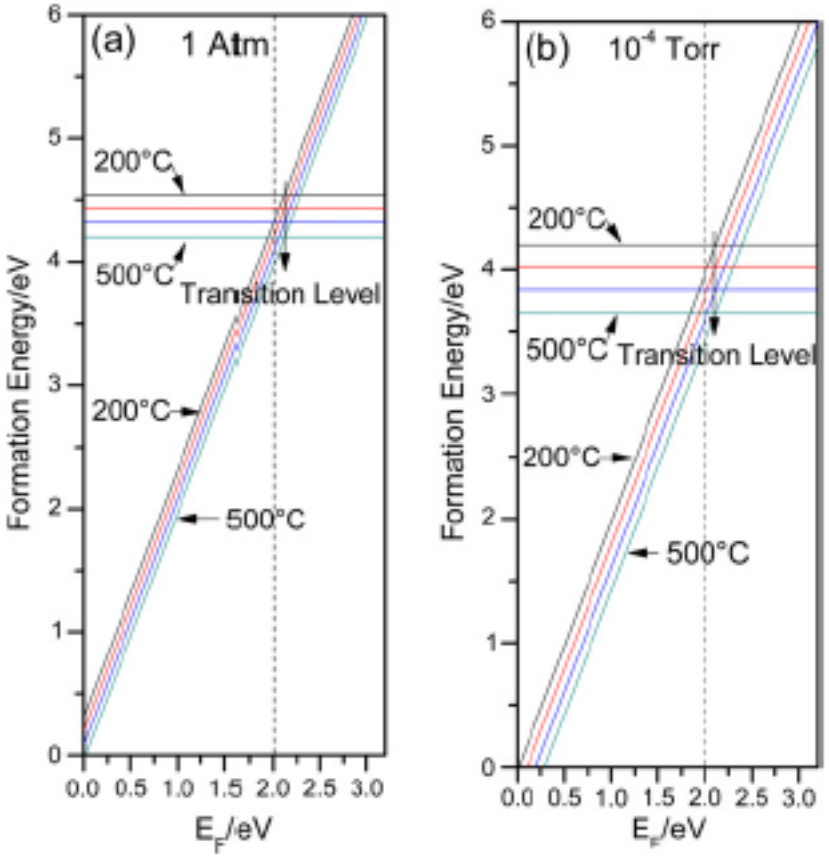
(a) 1 Atm
200°C
500°C
Transition Level
200°C
500°C
Formation Energy/eV
E_F/eV
(b) 10^-4 Torr
200°C
500°C
Transition Level
200°C
500°C
Formation Energy/eV
E_F/eV

Figure 2

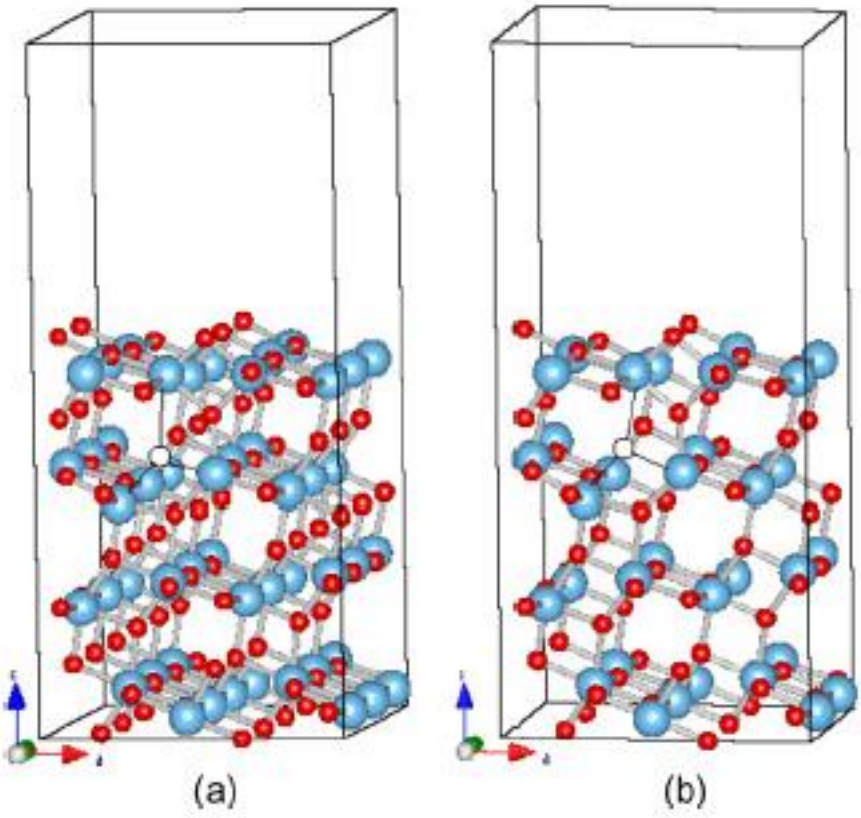

Figure 3

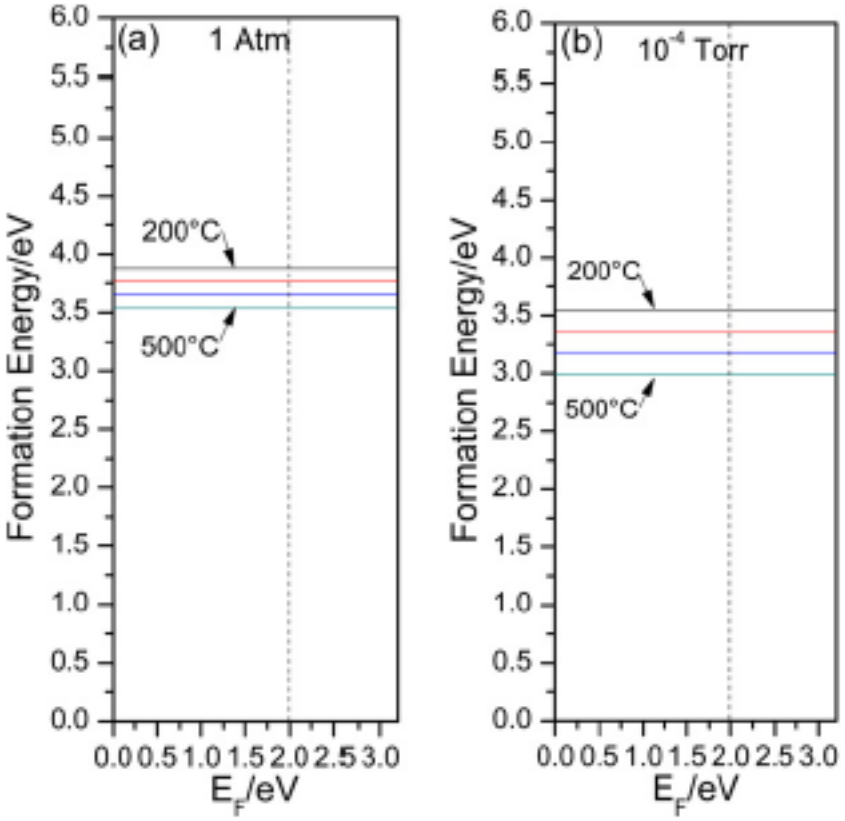

Figure 4

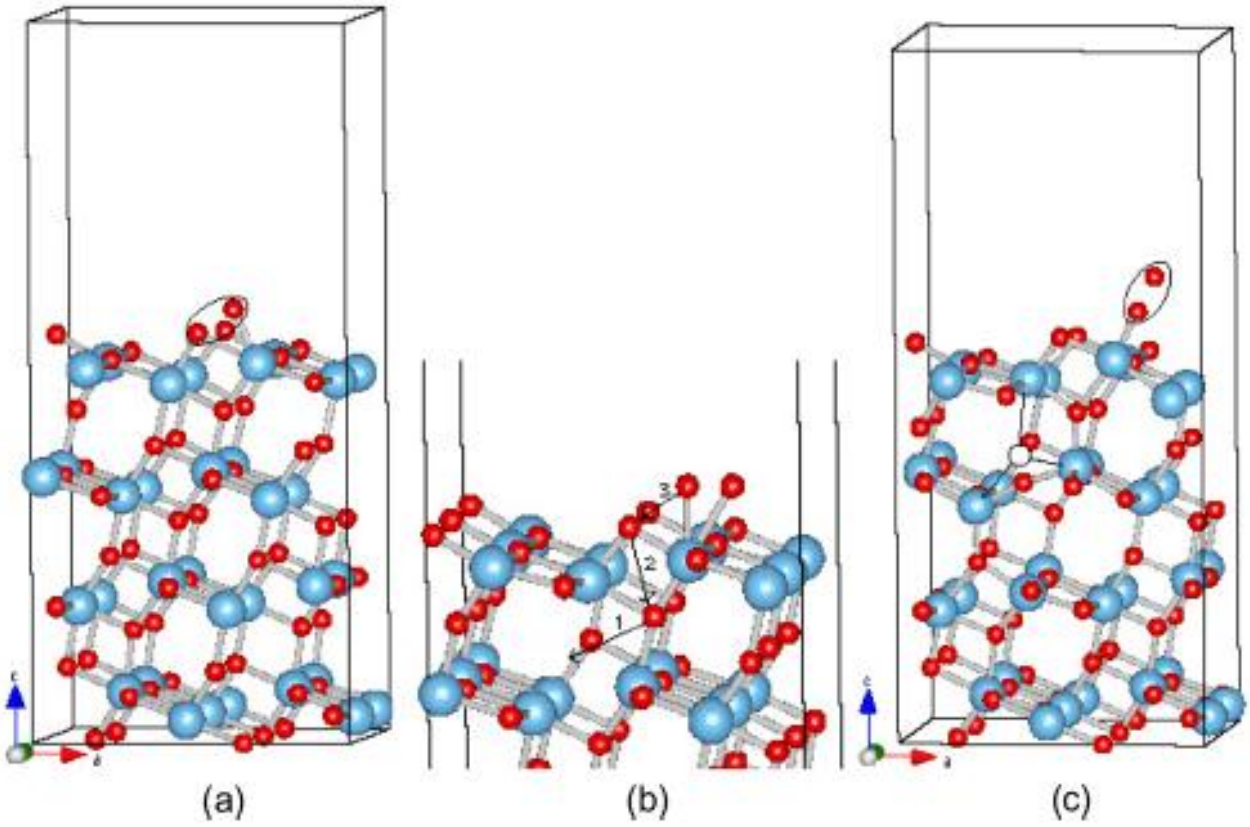

Figure 5

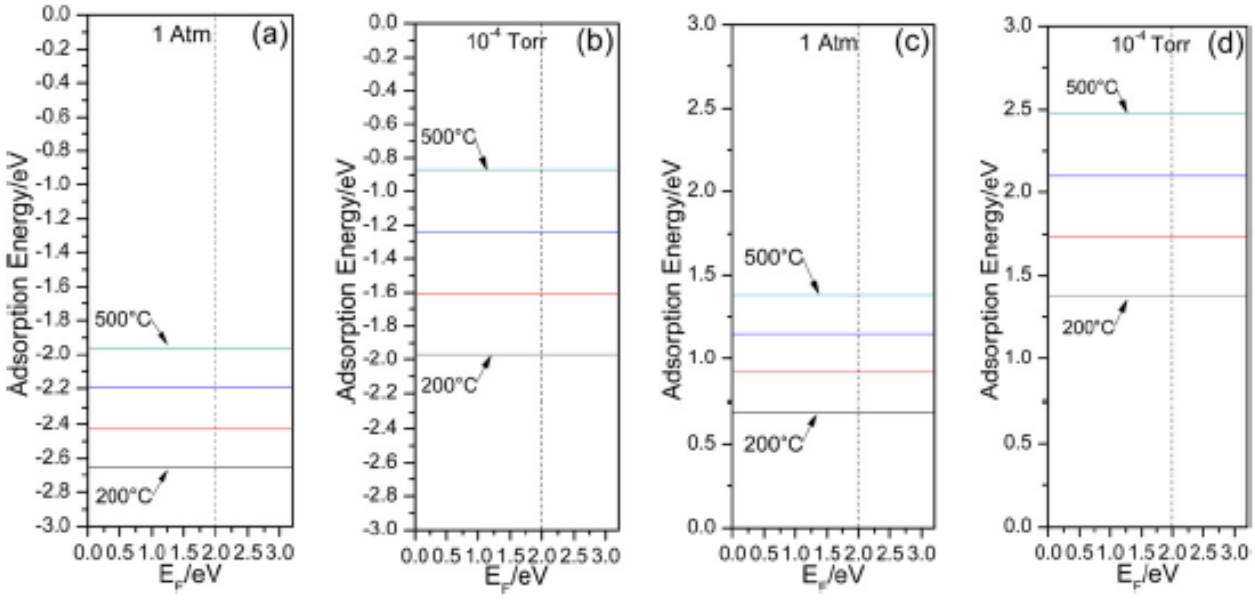

Figure 6

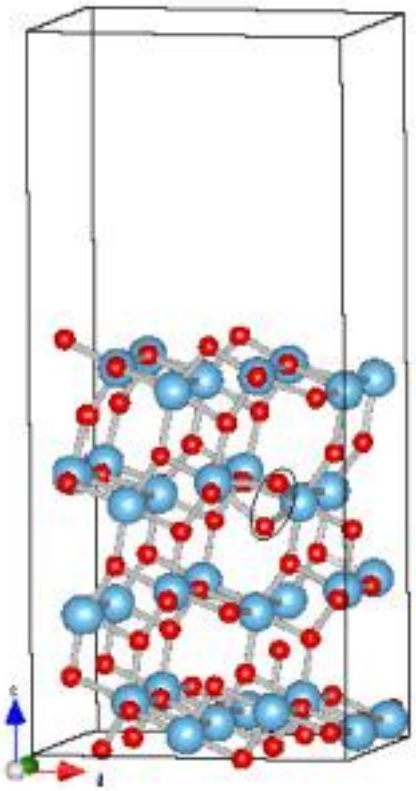

Figure 7

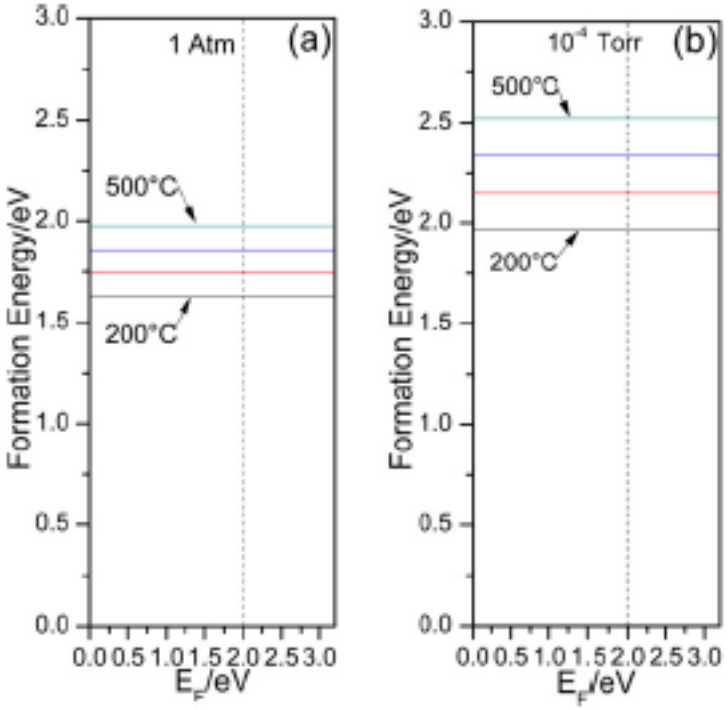

Figure 8

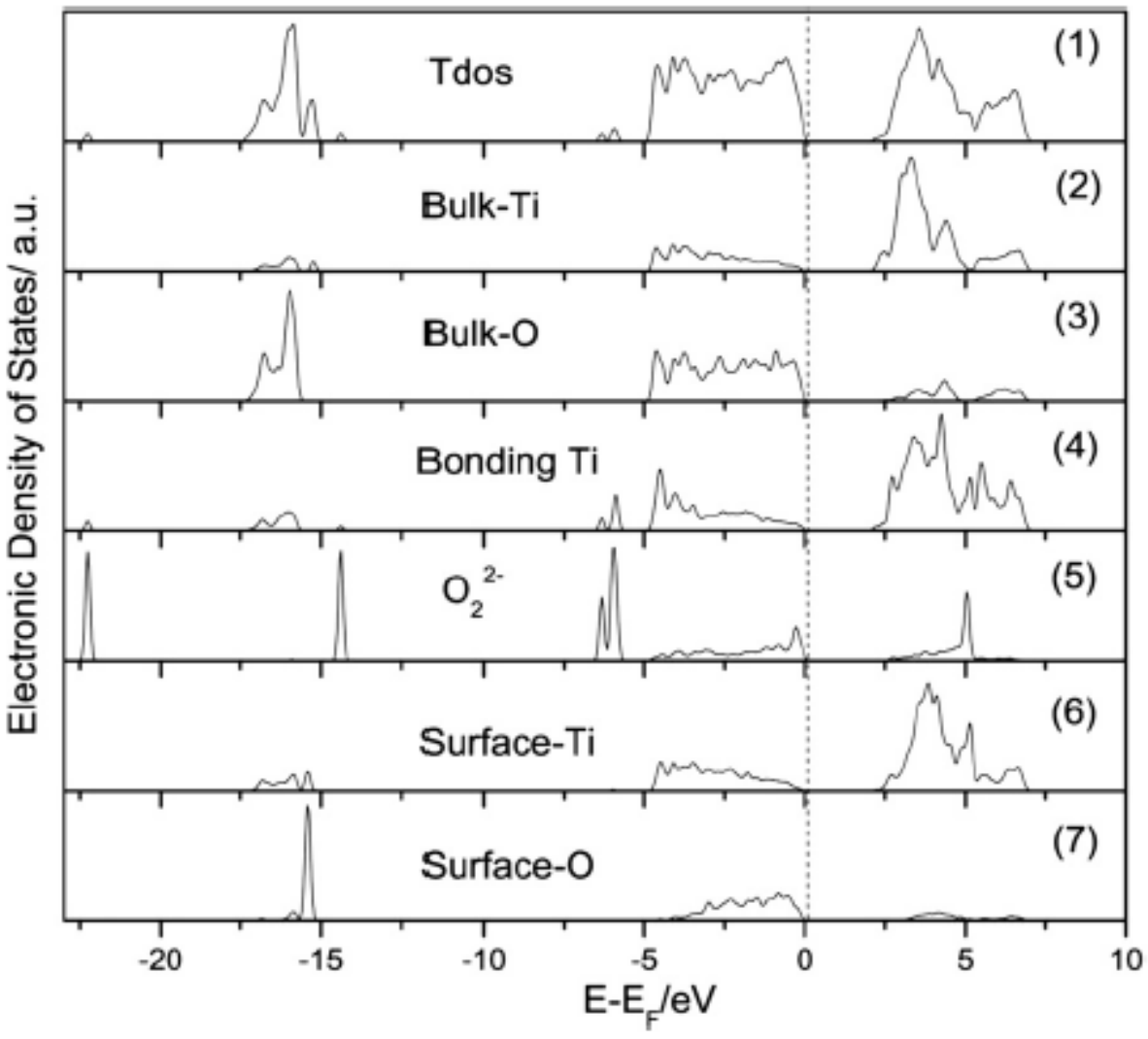
Tdos
(1)
Bulk-Ti
(2)
Bulk-O
(3)
Bonding Ti
(4)
O_2^{2-}
(5)
Surface-Ti
(6)
Surface-O
(7)
Electronic Density of States/ a.u.
-20
-15
-10
-5
0
5
10
E-E$_F$/eV

Figure 9